Autofluorescent Proteins in Single-Molecule Research: Applications to Live Cell Imaging Microscopy

Gregory S. Harms, Laurent Cognet, Piet H. M. Lommerse, Gerhard A. Blab, and Thomas Schmidt
Department of Biophysics, Leiden University, Leiden, The Netherlands

ABSTRACT The spectral and photophysical characteristics of the autofluorescent proteins were analyzed and compared to flavinoids to test their applicability for single-molecule microscopy in live cells. We compare 1) the number of photons emitted by individual autofluorescent proteins in artificial and in vivo situations, 2) the saturation intensities of the various autofluorescent proteins, and 3) the maximal emitted photons from individual fluorophores in order to specify their use for repetitive imaging and dynamical analysis. It is found that under relevant conditions and for millisecond integration periods, the autofluorescent proteins have photon emission rates of ~3000 photons/ms (with the exception of DsRed), saturation intensities from 6 to 50 kW/cm^2, and photobleaching yields from 10^{-4} to 10^{-5}. Definition of a detection ratio led to the conclusion that the yellow-fluorescent protein mutant eYFP is superior compared to all the fluorescent proteins for single-molecule studies in vivo. This finding was subsequently used for demonstration of the applicability of eYFP in biophysical research. From tracking the lateral and rotational diffusion of eYFP in artificial material, and when bound to membranes of live cells, eYFP is found to dynamically track the entity to which it is anchored.

INTRODUCTION

Research in the post-genomic era will be enhanced by applications of emerging physical techniques with modern biological methodology. One technique, which is believed to have a great impact in the endeavor to understand the way proteins function, is single-molecule microscopy (Weiss, 1999). For its application the protein under investigation has to be labeled specifically by an appropriate fluorescence tag. There is a large variety of labeling methods for proteins available applicable to in vitro assays (Hauglund, 1996), including several new developments utilizing semiconductor quantum dots (Bruchez et al., 1998; Chan and Nie, 1998) and highly photostable fluorophores (Holtrup et al., 1997). However, for labeling in the in vivo situation, utilization of those optimized fluorescence labels is limited. One of the most convenient, common, and benign ways to specifically label proteins in vivo is to construct a fusion with an autofluorescent protein from the jellyfish *Aequoria victoria* or one of its variants (Tsien, 1998). This methodology has the apparent advantage, compared to standard labeling with fluorescent dyes, of permitting the observation of dynamic processes in living systems (Tsien, 1989), with the hope of least interference with the biological function and vitality of the cell. The most recent approaches that combine genetic modification with the highly optimized properties of the new fluorophores are still waiting for their completion (Griffin et al., 1998). The combination of single-molecule microscopy with genetic labeling by autofluorescent proteins is the method we address in this article.

In the past, autofluorescent proteins have been progressively used for both in vivo and in vitro studies of cellular processes (Sullivan and Kay, 1999). By fusion to other proteins they are used as reporters of localization (De Giorgi et al., 1999), gene expression (Moriyoshi et al., 1996), trafficking, and in research on, e.g., ion channels (Zuhlke et al., 1999) and motor proteins (Iwane et al., 1997). The sensitivity of their fluorescence to the local environment has been further used to monitor local pH (Kneen et al., 1998) and local Ca^{2+} concentrations (Miyawaki et al., 1997). For the latter a unique Ca^{2+} sensor-protein, the chameleon system, has been developed (Miyawaki et al., 1997). Point mutations of the wild-type gene of *Aequoria victoria* resulted in a variety of proteins of different colors, the blue- (eBFP), cyan- (eCFP), green- (eGFP), and yellow-fluorescent proteins (eYFP) (Tsien, 1998). Recently, a gene encoding a red-fluorescent protein (DsRed) (Matz et al., 1999) was isolated from the reef coral, *Discosoma* sp. In parallel to those developments for cell biology the spectroscopic properties of autofluorescent proteins have attracted much attention and have been extensively described on the bulk level (Piston et al., 1999) for quantitative standard biological assays. Studies at the level of individual autofluorescent proteins were generally limited to the in vitro situation, where the purified protein was immersed in buffer (Widengren et al., 1999; Schwille et al., 1999) and biocompatible matrices (Dickson et al., 1997; Kubitscheck et al., 2000; Peterman et al., 1999; Schwille et al., 2000; Jung et al., 2000; Garcia-Parajo et al., 1999). Those studies have revealed anomalous properties such as reversible photobleaching (Dickson et al., 1997) and "blinking" (Garcia-

Received for publication 24 October 2000 and in final form 5 February 2001.

Address reprint requests to Dr. Thomas Schmidt, Dept. of Biophysics, Huygens Laboratory, Leiden University, Niels Bohrweg 2, 2333 AC Leiden, The Netherlands. Tel.: 31-71-527-5982; Fax: 31-71-527-5819; E-mail: tschmidt@biophys.leidenuniv.nl.

G. S. Harms's present address is Pacific Northwest National Laboratories, MSIN, Richland, WA 99352.

L. Cognet's present address is CPMOH-CNRS/Université Bordeaux I, 351 cours de la libération, 33405 Talence, France.

0006-3495/01/05/2396/13 $2.00

Parajo et al., 1999), which have remained undiscovered in previous bulk studies.

In comparison to the in vitro studies, the combination of single-molecule microscopy in a living cell, with the autofluorescent proteins or common fluorescence dyes (Sako et al., 2000; Schütz et al., 2000) has proven to be more delicate. This is mainly due to interference of the single-molecule fluorescence signal with background fluorescence created by other cellular constituents. In the visible region, the background mostly originates from flavinoids. Detailed knowledge about the spectroscopic properties of the autofluorescent (fusion-) proteins in comparison to those of the background is a prerequisite that will ultimately lead to optimized strategies for biophysical studies with autofluorescent fusion-proteins at the single-molecule level in living cells.

The current study reports the photophysical parameters of the commercially available autofluorescent proteins essential for single-molecule research. The measurements are performed in a way pertinent for in vivo single-molecule studies in cell biology, i.e., when anchored to artificial and to cell membranes by either a lipid anchor or when expressed as a fusion protein that is targeted to the cell membrane. The results are successfully compared to theoretical estimates taking results from bulk studies as a basis. That knowledge has allowed us to fine-tune our experimental parameters and demonstrate the utilization of autofluorescence proteins for single-molecule research in living cells (Harms, G. S., L. Cognet, P. H. M. Lommerse, G. A. Blab, H. Kahr, R. Gamsjäger, H. P. Spaink, N. M. Soldatov, C. Romanin, and T. Schmidt. Submitted for publication). More generally, those values will be the solid basis for identification of single-molecule events in complex systems, such as cells. Additionally, the following questions are addressed: 1) how do the autofluorescent protein variants compare for utilization in single-molecule research, and 2) under what conditions could individual fluorescent proteins be observed? The parameters, as reported here, show limits of utilization that will be discussed throughout the manuscript.

MATERIALS AND METHODS

Autofluorescent proteins

Plasmids containing the coding sequences of the fluorescent proteins (XFPs) under control of the *lac* promoter were obtained from Clontech (peCFP) or constructed (replacing eCFP in the Clontech plasmid by eGFP F64L/S65T or eYFP S65G/S72A/T203Y) (Clontech, Palo Alto, CA). A sequence encoding the His_6-tag was inserted at the 3′ end of the coding sequences of each XFP. The DNA was checked by restriction enzyme digestion and sequencing analysis. Subsequently, the plasmids were transformed into *Escherichia coli* SG13009 (Qiaexpress system, Qiagen, Hilden, Germany). Cultures of transformants were grown to OD620 $\approx$ 0.6 at 37°C and supplemented with isopropylthiogalactoside to a final concentration of 2 mM to induce XFP-His_6 production. After culturing for another 4 h at 37°C the cells were harvested by low-speed centrifugation. The cell pellet was washed and re-suspended in binding buffer (500 mM NaCl, 5 mM imidazole, 20 mM Tris-HCl pH 7.9) and lysis was performed by french-press. After 30 min of centrifugation at 15,000 $\times$ *g* a clear, colored supernatant was obtained. From the clear supernatant the His-tagged fluorescent proteins were purified using a column of Chelating-Sepharose-Fast-Flow (Pharmacia Biotech, Uppsala, Sweden) using a protocol outlined in the column manual. After elution the purified protein was dialyzed against phosphate buffered saline (PBS: 150 mM NaCl, 15 mM Na_2HPO_4, pH 7.4) for 8 h. Concentrations of the fluorescent proteins were determined by measuring their absorption spectra. SDS polyacrylamide gel electrophoresis analysis revealed a correct molecular weight and an estimated purity of at least 95%.

Gels

Polyacrylamide gels were made to 5% (w/w) with a purified stock solution of 30% acrylamide/1% bis-acrylamide added to 0.1% *N*,*N*,*N*′,*N*′-tetramethylethylene diamide and a diluted solution of purified fluorescent protein in PBS. The gels were polymerized after addition of 0.1% of ammonium persulfate in a thin smooth layer on cleaned no. 1 glass slides.

Phospholipid membranes

Lipid mixtures of POPC (1-palmitoyl-2-oleoyl-*sn*-glycero-3-phosphocholine), DPPC (1,2-dipalmitoyl-*sn*-glycero-3-phosphocholine), and Ni:NTA-DOGS (1,2-dioleoyl-*sn*-glycero-3-{[*N*(5-amino-1-carboxypentyl)-iminodiacetic-acid]-succinyl} (nickel salt)) (Avanti Polar Lipids, Alabaster, AL) were made by dissolving the pure lipids in chloroform. The lipid solutions were dissolved in filtered PBS to a final concentration of 2–5 mg/ml. For vesicle fusion onto a glass support the method of Rinia et al. (2000) was followed. For fusion of vesicles to cell membranes we used a method similar to Schütz et al. (2000). Before incubation with a 50 nM solution of XFP-His_6 proteins the samples were charged with 5 mM Ni^{2+} for several minutes.

Single-molecule imaging

The experimental arrangement for single-molecule imaging has been described in detail previously (Schmidt et al., 1995) (see also Fig. 1). Essentially, the samples were mounted onto an inverted microscope (Zeiss, Jena, Germany) equipped with a 100× objective (NA = 1.4, Zeiss, Jena, Germany), and illuminated for 5–10 ms by an Ar^+-laser (Spectra Physics, Mountain View, CA). Use of appropriate filter combinations (DCLP 550, HQ600/80; DCLP 498, HQ525/50; DCLP530, HQ570/80M (Chroma Technology, Brattleboro, VT), and GG495-3, OG515-3, OG530-3 (Schott, Mainz, Germany), holographic Super-Notch filter, 532 nm (Kaiser Optical, Ann Arbor, MI) permitted the detection of individual XFPs by a nitrogen-cooled CCD-camera system (Princeton Instruments, Trenton, NJ). The total detection efficiency of the experimental setup was between 0.05 and 0.12 depending on the fluorophore detected. The photon counts were determined with a precision of ~20%.

Fluorescence correlation measurements

Fluorescence correlation measurements were performed using a commercial system (ConfoCor, Zeiss, Jena, Germany). The excitation intensity was set between <1 and 20 kW/cm^2. The emission light was filtered by a 25-μm-diameter pinhole, and detected by an avalanche photodiode connected to a fast digital correlator. For timescales longer than 10 ms the correlation curves, $G(t)$, were fit by a combination of three-dimensional diffusion and photobleaching:

$$G_L(t) = N^{-1} \times (1 + t/t_d)^{-1}(1 + t/\omega^2 t_d)^{-1/2} \exp(-t/t_b),$$

where t_d is the mean diffusion time, t_b is the mean photobleaching time, N is the average number of fluorophores in the confocal volume, and ω is the length to diameter ratio of the confocal volume ($\omega = 5$). On the short timescale the correlation curve was fit to a three-state model including the triplet-, protonated- and dark-state (Widengren et al., 1999; Schwille et al., 1999):

$$G_S(t) = \prod_{i=1}^{3} 1 + f_i/(1 - f_i)\exp(-t/\tau_i),$$

yielding the lifetimes, τ_i, and occupations, f_i, respectively.

RESULTS

Single-molecule characterization

There is a general concurrence that observation of a single-molecule fluorescence event goes along with a fourfold of specific signatures, all based on the quantum mechanical nature of the fluorescence from an individual emitter (Weiss, 1999; Dickson et al., 1997; Basché et al., 1995; Schmidt et al., 1995): 1) the detected signal level for a given excitation rate and detection efficiency should be well defined, 2) the signal exhibits a characteristic one-step photobleaching behavior, 3) the detected fluorescence is polarized due to the well-defined transition dipole moment of the emitter, and 4) the signal is anti-correlated at time scales shorter than the fluorescent lifetime, an observation called photon anti-bunching (Basché et al., 1992).

In Fig. 1 our experimental setup and the above-mentioned criteria (1–3) are illustrated for the example of individual eYFP proteins being immobilized to a solid phospholipid membrane (from DPPC) via an Ni:NTA-lipid (Fig. 1 *A*). The images were obtained by wide-field fluorescence microscopy with localized signals, described by two-dimensional Gaussian surfaces, yielding values for the integrated fluorescence and the lateral position on the membrane. Subsequent positional tracking follows those signals over time at a rate of up to 20 images/s (see Methods for more details). Fig. 1 *B* (*top*) compares the signal of an individual eYFP molecule (diffraction-limited image with a width of 1.6 ± 0.2 pxl $= 320 \pm 30$ nm full-width-at-half-maximum and a signal amplitude of 170 ± 32 cnts) illuminated at an intensity of 5 kW/cm^2 for 5 ms with that of the fluorescence background of the phospholipid membrane (24 cnts root-mean-square). After a total illumination time of 30 ms the integrated signal level suddenly dropped from a mean of 162 ± 20 cnts for all six images to zero; a one-step photobleaching event occurred (Fig. 1 *B*, *bottom*). Further analysis of similar observations for a total number of 527 molecules yielded the fluorescence intensity distribution function and the photobleaching statistics for individual eYFPs shown in Fig. 1 *C*. The fluorescence intensity distribution function was constructed taking into account the value of the integrated fluorescence signal from individual molecule observations (as shown in Fig. 1 *B*), and its confidence level as obtained by a fitting procedure (Schmidt et al., 1995). The distribution is close to a Gaussian with a mean of 177 ± 20 cnts and a width of 63 ± 5 cnts. The width is mostly accounted for by the shot-noise and the instrument read-out noise of 8 cnts/pxl. The Gaussian intensity distribution with defined width indicates the "quantized" nature of the fluorescence intensity due to a single-molecule emitter. The single-molecule intensity distribution is compared to the background statistics shown as a dotted line in Fig. 1 *C* (*top*).

Evaluation of the time-until-photobleach statistics is shown in Fig. 1 *C* (*bottom*). For further characterization the data were fit to a monoexponential, yielding a mean photobleaching time of 3.8 ± 0.4 ms for the experimental parameter used in Fig. 1, *A*--*C*. Polarization imaging (Harms et al., 1999) was used to further demonstrate the defined transition-dipole moment of the signals and to analyze the rotational mobility of the autofluorescent proteins (Fig. 1 *D*). Whereas in the top of Fig. 1 *D* the emission from the eYFP was fully polarized in the s-direction (right column), it became almost entirely p-polarized (left column) after 320 ms, which suggests a slow rotational mobility. A discussion of the lateral and rotational dynamics of such membrane-anchored proteins will be presented later in detail. Demonstration of photon anti-bunching would be a quantum-mechanical indication of a single-molecule emitter which, due to the fast photobleaching behavior, proved to be prohibitively difficult for the autofluorescent proteins. Lastly, we have complemented our findings of single-molecule imaging with results from confocal fluorescence-correlation spectroscopy (Eigen and Rigler, 1994), which will be presented below.

Signal levels, saturation intensities, and photobleaching behavior of autofluorescent proteins in vitro

In this subsection the basic photophysical parameters of the autofluorescent proteins, the saturation intensity (I_s), the photobleaching time limit (τ_{bl}^{∞}), and the maximal photon emission rate (k_∞) are discussed. In addition to single-molecule experiments, all data have been complemented by results obtained on high-concentration (>100 nM) samples.

The photo-induced chemical destruction of the fluorescent entity is perhaps the most prominent quantity for single-molecule fluorescence research (Hirschfeld, 1976). This process limits the total number of photons one is able to yield from a fluorophore. We have determined the photobleaching time limit (τ_{bl}^{∞}), the time it takes the fluorophore to undergo photobleaching at infinite excitation intensity, from our single-molecule experiments. For this, individual autofluorescent proteins that have been either in solution or immobilized in polyacrylamide gel, or in the water-filled pores of a polyvinyl alcohol film, were observed for a series of excitation intensities between 0.5 and 120 kW/cm^2 and

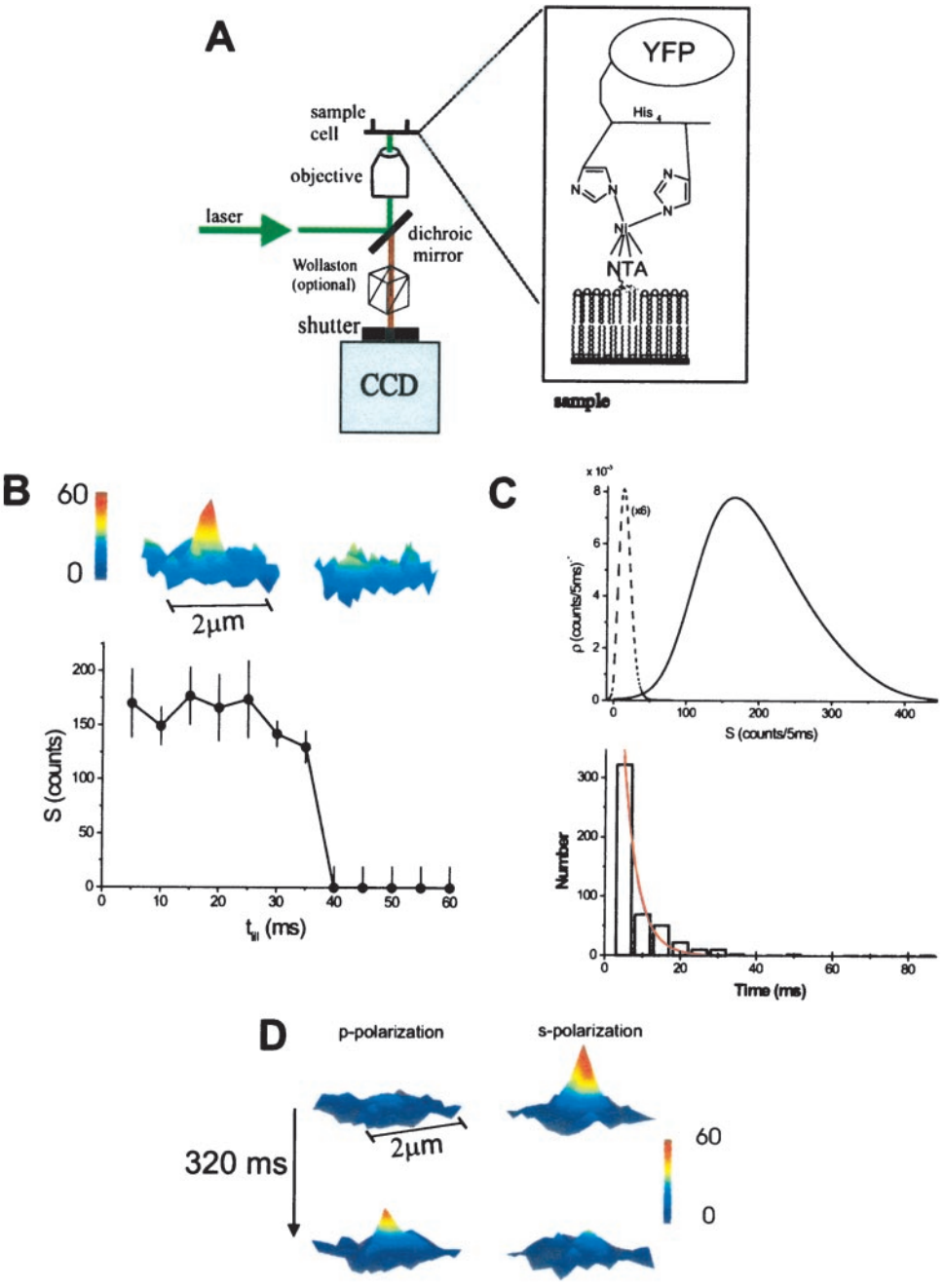

FIGURE 1 (*A*) Diagram of the widefield fluorescence microscope and the sample of eYFP-His_6 bound to a Ni^{2+} chelator on a supported phospholipid membrane. (*B*) *Top:* 2×2 μm^2 fluorescence image of an individual eYFP anchored to a DPPC membrane via a Ni^{2+}-NTA:DOGS lipid. The sample was excited with 514 nm laser light for 5 ms at 5 kW/cm^2. The signal of the background after the molecule has photobleached after 35 ms of illumination is shown for comparison. *Bottom:* Time trace of the single-molecule fluorescence signal. (*C*) *Top:* Statistical analysis of the fluorescence signal obtained from individual eYFP chelated to the lipid when illuminated by 5 kW/cm^2 at 514 nm. The probability density of the 527 signals analyzed is nearly Gaussian-shaped with a maximum at 177 cnts/5 ms. The statistics of the background is shown for comparison (*dashed line*). *Bottom:* Analysis of the photobleaching characteristics of 527 signals. On average the lifetime of eYFP is 3.8 ms as obtained by an exponential fit to the data (*solid line*). (*D*) Two consecutive polarization images of an individual eYFP anchored to a solid DPPC membrane via a Ni^{2+}-NTA:DOGS lipid. The sample was illuminated for 5 ms by circular polarized light. The data show the defined direction of the transition dipole moment characteristic for a single molecule, which slowly turns. (Delay between top and bottom images is 320 ms.)

for illumination times between 0.5 and 50 ms. First, from image sequences taken at one excitation intensity, a histogram of time-until-photobleach was constructed (as exemplified for eYFP in Fig. 1, *B* and *C*) and fit to a monoexponential decay ($\propto \exp(-t/\tau bl$, see Fig. 1 *C bottom*). The latter is characterized by a mean photobleaching time τ_{bl} ($\tau_{bl} = 3.8 \pm 0.4$ ms in the example in Fig. 1 *C*). The dependence of τ_{bl} on the excitation intensity, *I*, follows from a standard energy level model of a fluorophore (Lakowicz, 1999) (consisting of a ground state, multiple excited states, and a photobleached state, which is populated via the excited states). For such a model the intensity-dependent photobleaching time is given by $\tau_{bl}(I) = \tau_{bl}^{\infty}(1 + I_S/I)$, with the photobleaching time limit, τ_{bl}^{∞}, and the saturation intensity, I_s. These values were determined for various excitation intensities as shown in Fig. 2, *A*--*D* for eGFP and eYFP in a buffer and gel, eYFP immobilized on a phospholipid membrane, and DsRed in a gel. Additional fluorescence correlation spectroscopy (FCS) was performed on eYFP in polyacrylamide gels. Two such FCS data sets for two different excitation intensities of 0.6 and 4 kW/cm^2 are shown in Fig. 2 *E*. The mutual dependence on the photobleaching time with excitation intensity is clearly visible. Fitting the FCS curves (see Methods) yielded the photobleaching

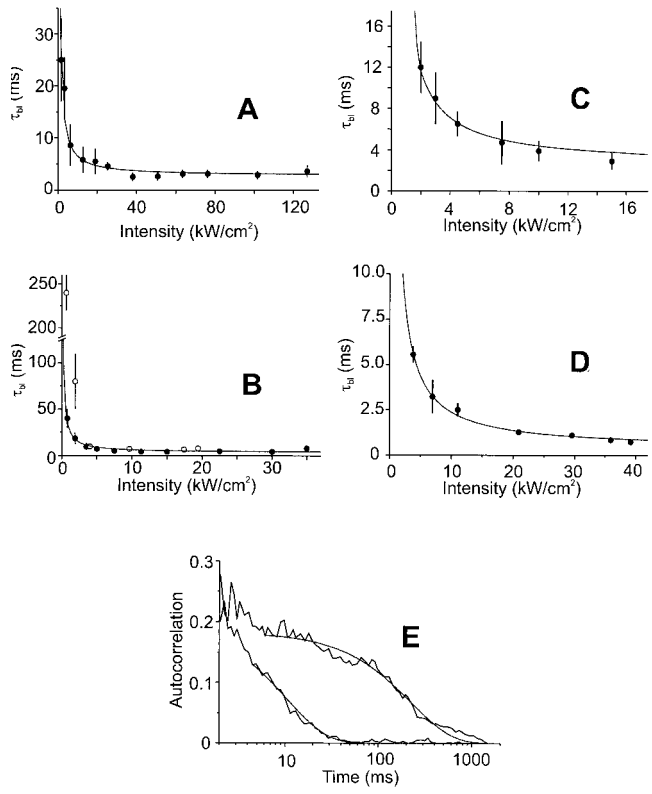

FIGURE 2 Mean photobleaching time, τ_{bl}, of individual fluorescent proteins (*filled circles*). The data were fit to Eq. 2 (*solid line*). (*A*) eGFP in PBS and in gel, $\tau_{bl}^{\infty} = 2.8$ ms. (*B*) eYFP in PBS and in polyacrylamide gel. Data obtained by correlation spectroscopy are shown as *open circles*. $\tau_{bl}^{\infty} = 3.5$ ms. (*C*) eYFP anchored to a phospholipid membrane, $\tau_{bl}^{\infty} = 2.6$ ms. (*D*) DsRed in polyacrylamide gel. $\tau_{bl}^{\infty} = 0.4$ ms. (*E*) FCS data-sets for two different excitation intensities of 0.6 (*right curve*) and 4 kW/cm^2 (*left curve*)

times, $\tau_{bl}(I)$, displayed in Fig. 2 *B* (*open symbols*), which closely resembles the data obtained by direct imaging. The data in Fig. 2, *A–D* follow the predicted behavior yielding the photobleaching time limit of $\tau_{bl}^{\infty} = 2.8 \pm 0.2$, 3.5 ± 0.5, 2.6 ± 0.1 ms, and 0.4 ± 0.1 ms for eGFP and eYFP in buffer and gel, eYFP on a phospholipid membrane, and DsRed in a gel, respectively. The values are ~10 times faster than those reported for synthetic fluorophores typically used in single-molecule research (Widengren et al., 1999; Schmidt et al., 1996).

Complementary imaging experiments have been performed for high-concentration (>100 nM) samples in which the purified proteins had been immersed in polyacrylamide gels. Table 1 lists photobleaching times and photobleaching yields for all of the fluorescence proteins observed as singles and at high concentration. The longer appearance of the bulk photobleaching times are due to the individual fluorescent proteins that start the scanning period in a nonfluorescent state (Peterman et al., 1999) and also by the smaller percentage of molecules that recover from photobleaching that would average out in time much of the true nonrecoverable photobleaching by molecules. In essence, the photobleaching time of a single molecule is defined by the true period of emission, whereas in bulk the start time is defined at the start of the illumination for the recording period and can be biased by delay in emission of some of the molecules, which has been determined to be true for a majority of eGFPs (Peterman et al., 1999).

A further significant quantity for the design of single-molecule experiments is the signal level one can expect for a given experimental arrangement. Besides the detection efficiency for a specific experimental setup, η_{det}, the signal level is dependent on the integration time, the excitation intensity and wavelength, the chemical environment, and finally limited by the photobleaching yield. Taking into account these parameters, the detected signal, S_{det}, as a function of excitation intensity, I, and integration time, t, is given by:

$$S_{det}(I, t) = \eta_{det} k_{\infty} \tau_{bl}^{\infty} \left[1 - \exp\left(\frac{-t}{\tau_{bl}^{\infty}(1 + I_S/I)} \right) \right] \quad (1)$$

with the saturation intensity, I_S, and the maximum photon emission rate, k_{∞}. In the case when photobleaching is negligible (i.e., $\tau_{bl}(I) \gg t$), the equation converts into the well-known form,

$$S_{det}(I, t) = \frac{\eta_{det} k_{\infty} t}{1 + I_S/I}.$$

(Demtröder, 1988). Fig. 3 depicts the intensity-dependent fluorescence obtained for individually observed eGFP and eYFP in a gel, attached to a phospholipid membrane and to DsRed in a gel. The data shown are obtained by determining the positions of the maximum of the fluorescence probability density (Fig. 1 *C*) for each excitation intensity. As stated earlier, those most probable values, S_{det}, depend on the integration time and the detection efficiency. In order to obtain generalized values that are not dependent on the specific experimental parameters, and hence easily comparable for each particular experiment, the data presented are corrected for the detection efficiency and illumination time effects. Such a generalized quantity is represented by the fluorescence rate of the molecule, F:

$$F(I) = \frac{S_{det}}{\eta_{det} \tau_{bl}(I)(1 - \exp(-t/\tau_{bl}(I))} = \frac{k_{\infty}}{1 + I_S/I}. \quad (2)$$

The fluorescence rate has been determined for eGFP, eYFP, and DsRed with excitation intensities between 0.5 and 120 kW/cm^2, as shown in Fig. 3. Fitting the data to the right-hand side of Eq. 2 yields the values for the maximum emission rate, k_{∞}, and the saturation intensity, I_S, as reported in Table 1.

TABLE 1 Photophysical properties of the autofluorescent proteins

	λ_{exc} (nm)	I_s (kW/cm^2)	k^∞ (photons/ms)	τ_{bl}^∞ (ms)	ϕ_{bl} ($\times 10^{-5}$)
eCFP					
high concentration	458	48 ± 12	2270 ± 300*	25 ± 2†	
single-molecule, gel	458		6000 ± 3000‡	<1	>19
eGFP					
high concentration	488	19 ± 6	2810 ± 300*	51 ± 2†	
single-molecule, gel	488	13 ± 3	2900 ± 200	2.8 ± 0.2	6.9 ± 0.5
eYFP					
high concentration	514	12 ± 3	3320 ± 300*	112 ± 3†	
single-molecule, gel	514	6 ± 1	3100 ± 100	3.5 ± 0.5	5.5 ± 0.5
single-molecule, membrane	514	9 ± 2	3100 ± 300	2.6 ± 0.1	7.2 ± 0.5
DsRed					
high concentration	532	45 ± 10	12500 ± 200*	0.3 ± 0.1†	
single-molecule, gel	532	50 ± 10	18000 ± 2000	0.4 ± 0.1	15 ± 3
flavin					
high concentration	514	35 ± 10	500 ± 100		

*Calculated from the mean signal in a 4 × 4 μm^2 area and assuming an imaged volume of 0.1 fl/pixel.
†Taken as the mean from a multiexponential decay.
‡From a wide distribution of data. The photobleaching was so rapid that I_S was impossible to determine.

Those data derived from single-molecule observations have been subsequently compared to values attained at high concentrations (>100 nM). The data in Table 1 summarize the results of the average fluorescence count-rate obtained for a ~ 40 × 40 pxl image area. It should be noted that photobleaching was negligible due to short integration times (down to 50 μs) used in these experiments. The fluorescence signal for an individual molecule can be estimated from those measurements. The resemblance of the estimated signal per molecule with the actual single-molecule data gives confidence to our single-molecule results.

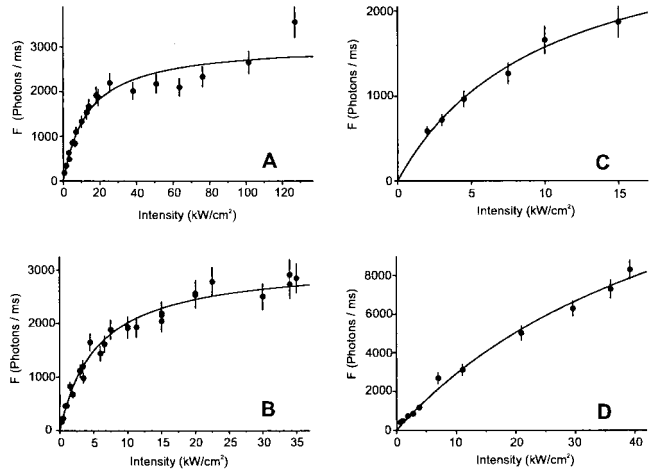

FIGURE 3 Single molecule fluorescence rate (Eq. 1) as a function of laser intensity. The data were fit to the right part of Eq. 2 (*solid lines*). (*A*) eGFP in PBS, I_s = 13.4 kW/cm^2 and k_∞ = 2900 photons/ms (λ_{exc} = 488 nm). (*B*) eYFP in PBS and in polyacrylamide gel, I_s = 5.5 kW/cm^2 and k_∞ = 3100 photons/ms (λ_{exc} = 514 nm). (*C*) eYFP anchored to a phospholipid membrane, I_s = 9.8 kW/cm^2 and k_∞ = 3100 ± 200 photons/ms (λ_{exc} = 514 nm). (*D*) DsRed in polyacrylamide gel, I_s = 50 kW/cm^2 and k_∞ = 18,000 photons/ms (λ_{exc} = 532 nm).

Comparing the different autofluorescent proteins, the results detailed above are summarized in Table 1. The maximum emission rate varies from k_∞ ~ 2270–18,000 photons/ms, the saturation intensity varies between 6 and 50 kW/cm^2, and the photobleaching times vary between τ_{bl}^∞ = 0.4 and 3.5 ms in aqueous environments, at pH 7.4, and at ambient temperatures. From the values it appears that the suitability of the autofluorescence proteins for single-molecule microscopy is given by eYFP > eGFP ≫ eCFP, leaving DsRed out of consideration. A detailed evaluation of that ranking will be specified in the Discussion section. Taking the superiority of eYFP all studies presented in the following subsections, focusing on cell biological aspects, were performed with eYFP as a fluorescence tag.

Utilization of eYFP for in vivo studies

Signal level of membrane-bound eYFP

Various fluorescence techniques have been applied to date to unravel the dynamics of physiological processes mostly utilizing synthetic fluorophores for labeling (Edidin, 1987; Saxton and Jacobson, 1997). Here we use individual eYFP molecules that were studied when bound to artificial phospholipid bilayers (see Figs. 2 *C* and 3 *C*) and membranes of live cells. The virtue of the eYFP in this field of research is that it can be used as a genetic tag and as a conventional fluorescence label utilizing simple linker chemistry. The purification step of eYFP (and other proteins) usually involves genetic modification of the protein with a histidine tag, giving a eYFP-His$_6$ construct. We utilized a phospholipid, DOGS, which carries a Ni^{2+}:NTA headgroup for specific immobilization of eYFP-His$_6$ proteins onto biomembranes.

First a fluid phospholipid membrane of a mixture of DOGS:Ni^{2+}:NTA and POPC (ratio 10^{-6} mol/mol) was prepared on a glass substrate, which is subsequently incubated with eYFP-His_6. The sparse density of DOGS:Ni^{2+}:NTA resulted in a very low coverage by eYFP-His_6 (<1 μm^{-2}). Before investigation of the mobility of the eYFP-His_6-Ni^{2+}:NTA:DOGS complex the photophysical implications of the Ni^{2+}:NTA group on the eYFP fluorescence signal were studied. Although electronic interactions are assumed to be a minimal influence of the doubly charged Ni^{2+} ion on the fluorescence properties of the eYFP, they could not be excluded, a priori. By comparison of the photophysical parameters of membrane-anchored (via Ni^{2+}:NTA) and free eYFP (Table 1) no significant difference is found in signal level and saturation intensity. The photobleaching rate of membrane-bound eYFP is increased by ~20% in comparison to eYFP in aqueous environment.

In the same way, eYFP was anchored to the plasma membrane of a live cell (Fig. 4 *A*). For this, human aorta smooth muscle cells (HASM) were incubated with a 0.5 mg/ml solution of vesicles containing DOGS:Ni^{2+}:NTA lipids (10^{-2} mol/mol). After washing in vesicle-free buffer and incubation with eYFP-His_6, the proteins were able to specifically immobilize onto the DOGS:Ni^{2+}:NTA lipids incorporated in the membrane of the cell. It is interesting to see (Fig. 4 *B*), that the signal level of eYFP immobilized onto the surface of a cell closely resembles that of eYFP when studied on an artificial membrane and when embedded in aqueous environment. Hence, utilization of eYFP for single-molecule in vivo studies seems possible. We have also been successful in the identification and the study of individual eYFPs fused to a membrane-targeting CAAX sequence, the α_{1C} subunit of the L-type calcium channel (Harms et al., submitted for publication), and to the kinase 14–3-3ζ in vivo. The experimental results of those fusion proteins will be described in detail in separate publications from our laboratory, but have been summarized in Table 2.

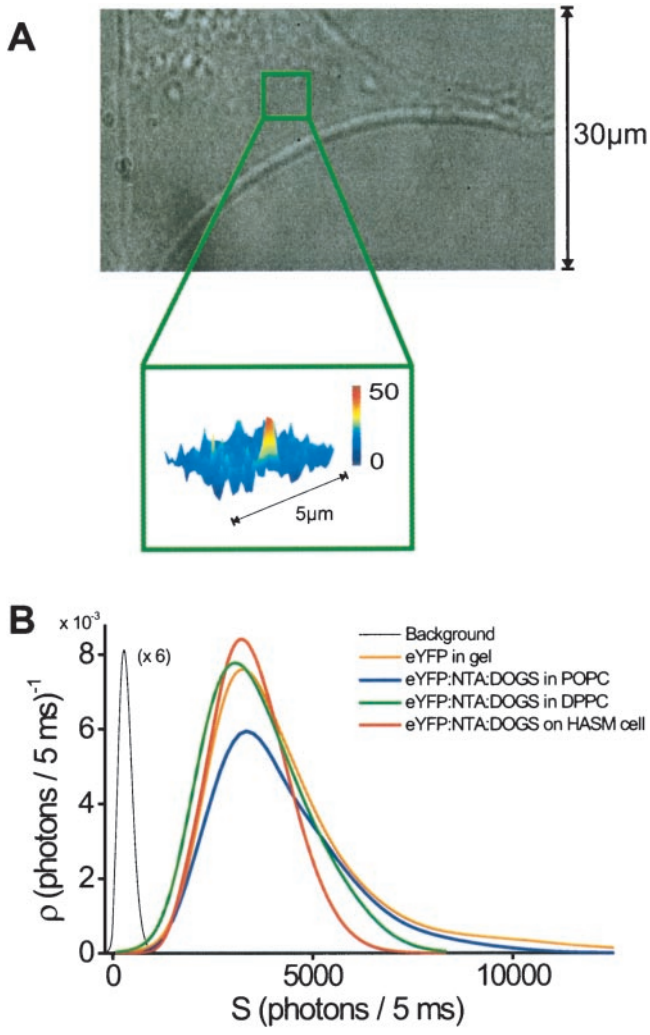

FIGURE 4 (*A*) White-light image of a human aorta smooth muscle cell and fluorescence image of an individual eYFP:NTA:DOGS lipid attached to this cell from the indicated region on the white light image. (*B*) Probability density of fluorescence emission signals obtained from individual eYFP-Ni^{2+}:NTA:DOGS lipids obtained for an excitation intensity of 5 kW/cm^2 and integration time of 5 ms with background signal labeled in black, 1) in the plasma membrane of HASM cells (*red*), 2) in a DPPC lipid membrane (*green*), 3) in a POPC lipid membrane (*blue*), and 4) when embedded a polyacrylamide gel (*orange*).

Mobility of individual free and membrane-anchored eYFP

Utilization of eYFP for single-molecule biophysical studies is demonstrated in this section. Individual eYFP-His_6-Ni^{2+}:NTA:DOGS lipid-protein complexes were followed at image rates between 20 and 100 Hz on 12 × 12 μm^2 areas in the various samples. From image sequences their trajectories were reconstructed. Each point of the trajectory was determined with an accuracy of <80 nm, limited by the signal-to-background-noise ratio of ≥15 in our experiments. This allowed us to sensitively follow the motions of the individual lipid-protein complexes. A few such trajectories are shown in the insets of Fig. 5. The mobilities were analyzed in terms of the distribution of lateral diffusion constants, D_{lat}, being calculated from the squared-displacement, sd, and lag time between two observations, t, for each individual protein (D_{lat} = sd/4t). The results are summarized in Fig. 5 and Table 3. The diffusion of eYFP in buffer solution is shown for comparison (for that, the projection of the three-dimensional trajectory onto the image plane was analyzed). All distributions follow the predicted exponential distribution (Chandrasekar, 1943) characterized by a mean diffusion constant of 8 ± 1 μm^2/s for free eYFP in buffer (Fig. 5 *A*), 1.96 ± 0.09 μm^2/s for the eYFP-His_6-Ni^{2+}:NTA:DOGS complex on a fluid POPC membrane (Fig. 5 *B*), < 0.01 μm^2/s for the eYFP-His_6-Ni^{2+}:NTA:DOGS complex on a solid DPPC membrane (Fig. 5 *C*), and 0.11 ± 0.04 μm^2/s for the eYFP-His_6-Ni^{2+}:NTA:DOGS on the plasma membrane of a living HASM cell (Fig. 5 *D*).

TABLE 2 Signal of single eYFP fusions in vivo

	λ_{exc} (nm)	I_{ex} (kW/cm^2)	Photons/ms	τ_{bl} (ms)	ϕ_{bl} ($\times 10^{-5}$)
eYFP-α_{1C} subunit in HEK cell	514	4.5	800 ± 200*	2.5 ± 0.5	3.8 ± 0.5
eYFP-CAAX in HEK cell	514	2	975 ± 100	4.5 ± 0.5	2.0 ± 0.5
eYFP-14-3-3 *Dictyostelium*†	514	3	1000 ± 200*	3.0 ± 0.5	3.0 ± 0.5

*Values are not corrected for photobleaching that occurred during the integration period.
†Values are from fixed cells.

It is interesting to note that the diffusion constants of the eYFP-His$_6$-Ni^{2+}:NTA:DOGS complex on the various membranes resembles that of the lipid anchor (Edidin, 1987). The bulky protein and linker group do not significantly disturb the mobility of the lipid. Hence, interaction of the autofluorescent proteins with the membrane is weak and probably does not interfere with the local organization of the lipid bilayer, nor is the protein itself partly incorporated into the membrane. This is verified by the results of the diffusion of similar, yet smaller, artificially labeled lipids in the same environment at the single-molecule level. It should be further noted that the observed diffusion constant of free eYFP in the control buffer solution is different from previously reported values of $\sim$ 80 μm^2/s (Widengren et al., 1999; Jung et al., 2000), which were identical to that predicted from the Stokes-Einstein equation assuming a globular shape of eYFP with radius $r = 0.25$ nm (Ormo et al., 1996) and viscosity of the buffer of 1 cPoise. The small diffusion constant found in our experiments for the buffer measurements are rationalized by the experimental restrictions valid here. In order to observe individual molecules in our setup they have to be in close proximity to the solid substrate. In this situation short adhesion events and the increased viscosity of the solvent close to the support will account for a smaller diffusion constant.

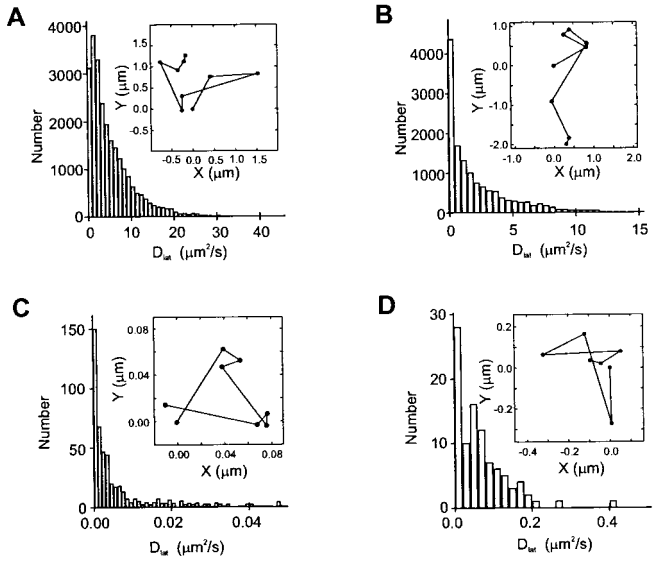

FIGURE 5 Histogram of the diffusion constant, $D_{lat} = SD/4\ t_{lag}$, calculated from single-molecule trajectories (*shown in the insets*). (*A*) eYFP in PBS, $\langle D_{lat}\rangle = 7.6$ μm^2/s. (*B*) eYFP-Ni^{2+}:NTA:DOGS lipid anchored to a POPC membrane, $\langle D_{lat}\rangle = 2.0$ μm^2/s. (*C*) eYFP-Ni^{2+}:NTA:DOGS lipid anchored to a DPPC membrane, $\langle D_{lat}\rangle$ 0.01 μm^2/s. (*D*) eYFP-Ni^{2+}:NTA:DOGS lipid anchored to the plasma membrane of a HASM cell, $\langle D_{lat}\rangle = 0.11$ μm^2/s.

The rotational mobility of free eYFP and the eYFP-His$_6$-Ni^{2+}:NTA:DOGS complex on the various lipid membranes was analyzed simultaneously with the lateral mobility by introduction (Table 3) of a Wollaston prism into the infinity beam-path of the microscope (Harms et al., 1999). For all samples a high mean fluorescence polarization, $\langle P\rangle = \langle (I_{||} - I_{\perp})/(I_{||} + I_{\perp})\rangle$, of 0.41 ± 0.06 (mean ± SE) was found on excitation with linear polarized light (see Fig. 6*A* for eYFP-His$_6$-Ni^{2+}:NTA:DOGS on the fluid POPC membrane). Control experiments with circularly polarized light yielded $\langle P\rangle = 0.03 \pm 0.05$. Given the large size of the protein, and hence its slow rotational diffusion time of $\tau_{rot} \sim 20$ ns (Widengren et al., 1999; Swaminathan et al., 1997), much longer than the fluorescence lifetime of $\tau_S = 3.7$ ns (Widengren et al., 1999; Schwille et al., 2000; Swaminathan et al., 1997), the high value of the polarization in a steady-state experiment has been predicted.

However, for solid DPPC membranes, the situation changes. The rotation of the eYFP-His$_6$-Ni^{2+}:NTA:DOGS complex in the solid membrane is slow enough in some cases that it could be directly visualized. An example of such a slowly rotating individual eYFP anchored to a DPPC membrane is shown in Fig. 6 *B*. Analysis of the mean-squared angular displacements of the transition dipole moment yields a mean rotational diffusion constant obtained

TABLE 3 Dynamics of eYFP linked to lipids or fused to proteins

	D_{lat} (μm^2/s)	Polarization ($\langle P\rangle$)*
eYFP-Ni^{2+}:NTA:DOGS-DPPC	<0.01	0.39 ± 0.07
eYFP-Ni^{2+}:NTA:DOGS-POPC	1.96 ± 0.09	0.39 ± 0.07
eYFP-Ni^{2+}:NTA:DOGS-HASM cell	0.11 ± 0.04	0.45 ± 0.05
eYFP-buffer	7.6 ± 0.5	0.33 ± 0.05
eGFP-buffer	7.6 ± 0.5	0.33 ± 0.05
eYFP-α_{1C} subunit in HEK cell	0.14 ± 0.05	
eYFP-CAAX in HEK cell	0.25 ± 0.06	

*On linearly polarized excitation; on circularly polarized excitation, $\langle P\rangle = 0.0 \pm 0.1$.

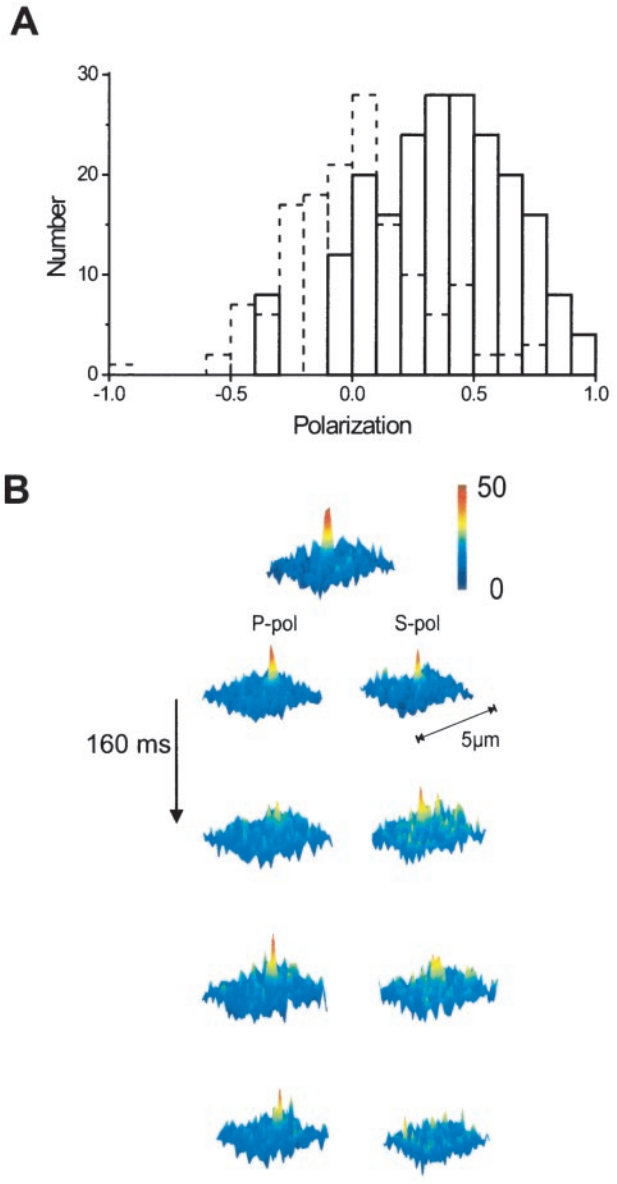

FIGURE 6 (*A*) Histograms of the polarization values determined from individual eYFP-Ni^{2+}:NTA:DOGS embedded in a fluid POPC membrane with linear (*solid lines*) and circular (*dashed lines*) polarized excitation. $\langle P_{lin}\rangle = 0.39$, $\langle P_{circ}\rangle = 0.02$. (*B*) Consecutive images of a 5×5 μm^2 DPPC membrane area with the signal from a single eYFP- Ni^{2+}:NTA:DOGS lipid. The delay between the images was 150 ms. Assuming that the transition dipole moment of the eYFP is aligned with the membrane plane, a rotational time of 100 ms is determined.

from 10 complexes of $D_{rot} = 3 \pm 1$ rad^2/s. Hence, as found for fluorescence-labeled lipids, the rotation of the fluorescent protein closely follows that of the lipid anchor in the solid membrane (Harms et al., 1999). This finding indicates that utilization of an Ni^{2+}:NTA linker to a fluorescent protein might be a valuable strategy for other rotational studies in, e.g., in vitro and in vivo protein dynamics using eYFP as a fluorescent tag.

DISCUSSION

The photophysics as predicted from a five-level system

We first present a theoretical model calculation that predicts both the saturation intensity, I_s, and the maximal photon emission rate, k_∞. The underlying model takes into account the four different forms the autofluorescent proteins can occupy (Widengren et al., 1999; Schwille et al., 2000; Jung et al., 2000; Creemers et al., 1999): a fluorescent bright form; a nonfluorescent protonated form, *P*; a nonfluorescent dark form, *D*; and a nonfluorescent photoproduct form. The bright form further consists of the fluorescent singlet state, *S*, a nonfluorescent triplet state, *T*, and a ground state, *G*, from which the photon absorption occurs (Fig. 7). Fluorescence saturation is due to the occurrence of a bottleneck owing to a slow, competing de-excitation mechanism of the excited singlet state, which limits the fluorescence rate (Lakowicz, 1999; Demtröder, 1988). The model presented in Fig. 7 sufficiently describes our observations. The photophysical rates connected to our model are the absorption cross section at the excitation wavelength, $\sigma(\lambda)$, the fluorescence quantum efficiency, Φ, the lifetime of the singlet state, τ_S, the rates connected to the triplet state, k_T, and its population channel via inter-system crossing, k_{ISC}. To account for the other forms of the proteins, effective rates are taken into account which characterize the population, k_{SP}, k_{SD}, k_{bl}, and depopulation k_P, k_D of the respective form (see Fig. 7). Assuming that the de-excitation of the singlet excited-state is governed by the singlet lifetime we obtain by

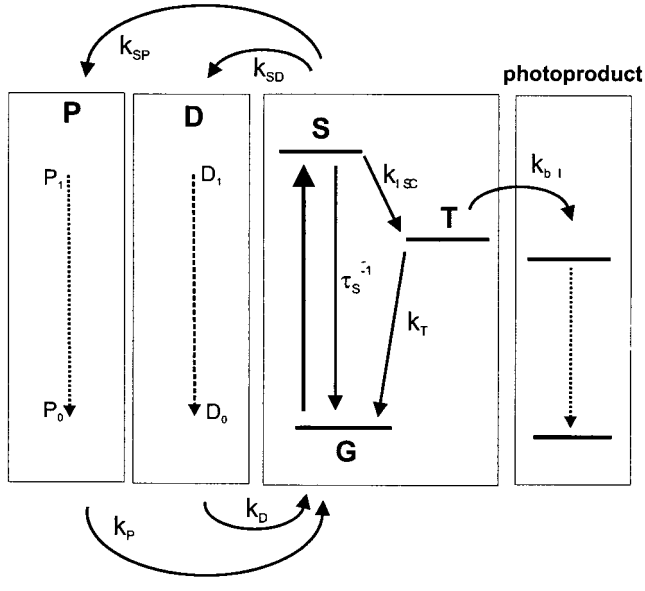

FIGURE 7 Rate and energy-level diagram of the fluorescent proteins. The ground state, *G*, singlet-excited state, *S*, triplet state, *T*, protonated form, *P*, and dark form, *D*, are taken into account. The states and forms are connected with the respective rate constants.

solving the steady-state rate equations:

$$I_S = \frac{hc}{\lambda\sigma(\lambda)} \frac{1/\tau_S}{1 + 1/f_T + 1/f_D + 1/f_P},$$

$$k_\infty = \frac{\Phi}{\tau_S(1 + 1/f_T + 1/f_D + 1/f_P)}$$

with the relative populations of the triplet state, $f_T = k_T/k_{ISC}$, the dark, $f_D = k_D/k_{SD}$, and protonated form, $f_P = k_P/k_{SP}$, respectively. The above-mentioned parameters f_T, f_D, and f_P were measured by us and others (Widengren et al., 1999; Schwille et al., 2000; Jung et al., 2000) using correlation spectroscopy on eGFP and eYFP. So far, characterization of the dark and protonated states, and the excited-state lifetime, have not been reported for eCFP. For eGFP, we predict $I_s = 29$ kW/cm^2 and $k_\infty = 8500$ photons/ms, given $\sigma(488\text{ nm}) = 1.7 \cdot 10^{-16}$ cm^2, $\Phi = 0.6$ (Tsien, 1998), $\tau_S = 3.2$ ns (Widengren et al., 1999), $f_T = 0.1$, $f_D = 0.2$, $f_P = 0.17$. For eYFP ($\sigma(514\text{ nm}) = 2.5 \cdot 10^{-16}$ cm^2, $\Phi = 0.6$ (Tsien, 1998), $\tau_S = 3.7$ ns (Widengren et al., 1999; Schwille et al., 1999; Swaminathan et al., 1997), $f_T = 0.08$, $f_D = 0.12$, and $f_P = 0.25$)) we obtain $I_s = 16$ kW/cm^2, $k_\infty = 6400$ photons/ms. Reports for DsRed indicate ($\sigma(532\text{ nm}) = 3.7 \cdot 10^{-17}$ cm^2, $\Phi = 0.29$ (Tsien, 1998), $\tau_S = 2.8$ ns (Jakobs et al., 2000) (and more recently: $\sigma(532\text{ nm}) = 1.1 \cdot 10^{-16}$ cm^2, $\Phi = 0.7$ (Baird et al., 2000), $\tau_S = 3.65$ ns (Heikal et al., 2000)), $f_T \sim 0.1$ (estimate) and $f_D \sim 0.1$ (estimate) such that we obtain $I_s \sim 170$ kW/cm^2, $k_\infty \sim 5000$ photons/ms (and $I_s \sim 56$ kW/cm^2, $k_\infty \sim 9000$ photons/ms with the more recently published values for σ, Φ, and τ_S). The figures are in reasonable agreement with those experimentally determined. It is interesting to note, for the rational assumption that the lifetime, quantum-yield, and effect of the dark state for the various autofluorescent proteins are on the same order, k_∞ should be similar for eCFP. Indeed, this has been verified by some of our experiments with eCFP. The largely increased count rate observed for DsRed leads to the conclusion that the rates connected to the model will fundamentally be different, as has been evidenced in a recent publication on the fluorescence lifetime of DsRed (Jakobs et al., 2000) and slow rotational time (Heikal et al., 2000) due to a plausible self-aggregation (Baird et al., 2000).

The definition of the system-independent, emitted photon rate when the molecule is in a fluorescent state does allow for a stringent comparison of the signal levels, independent of the actual detection efficiencies and possible differences in photobleaching rates and/or dark states. The observation of dark states that have been reported to occur on short (0.1–100 μs) (Widengren et al., 1999; Schwille et al., 2000; Garcia-Parajo et al., 1999) and long (0.1–10 s) (Dickson et al., 1997; Peterman et al., 1999) time scales complicates the interpretation of photobleaching data. In our experiments only a small population (<10%) of the autofluorescent proteins when immobilized exhibited recovery or "blinking"; however, there is an "off time" of 200 ± 50 ms for eYFP (Fig. 8), much like previously being attributed as anomalous behavior (Peterman et al., 1999) and agrees with the high-concentration photobleaching rate (Table 1). For a mobile sample the long-time recovery from a photobleached state is indistinguishable from diffusion. Taking the five-level system, the photobleaching efficiency, ϕ_{bl}, the probability for photobleaching per absorbed photon, is calculated from the photobleaching time limit by Peterman et al. (1999) and Schmidt et al. (1995):

$$\phi_{bl} = \frac{\tau_s}{\tau_{bl}^{\infty}}(1 + 1/f_T + 1/f_D + 1/f_P).$$

In our experiments, the photobleaching efficiencies for the different autofluorescence proteins at the single molecule level are within the range of $\phi_{bl} = 10^{-4}$ to $5 \cdot 10^{-5}$ (see Table 1). This value is in good agreement with that reported by other single-molecule measurements (Kubitscheck et al., 2000) and to values reported as a comparison with a conventional fluorophore (Tsien, 1998). The somewhat lower values found in Peterman et al. (1999) ($\phi_{bl} = 8 \cdot 10^{-6}$ for eGFP) could probably be accounted for by the longer integration times used in those experiments.

Autofluorescent proteins for the use in single-molecule studies in cells

The application of single-molecule studies to the research of in vivo systems has been mainly hampered by the autofluorescence observed in living cells. Cellular autofluorescence in the yellow-green region is chiefly due to the fluorescence of flavinoids, which are abundant in concentrations of 10^6-10^8 molecules/cell (Benson et al., 1979). One way to reduce

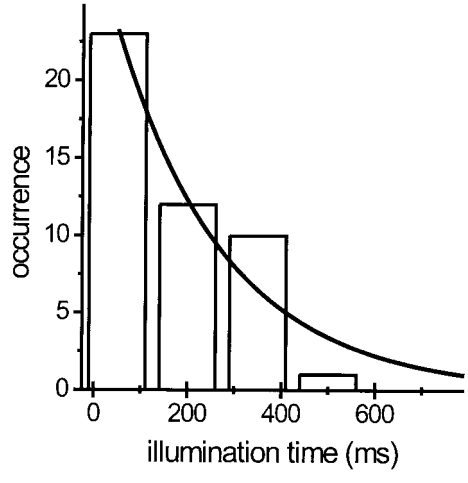

FIGURE 8 Off-rate histogram and single exponential fit as determined by the method of Peterman et al., 1999 for individual eYFP in a biocompatible polyacrylamide gel. Excitation was with 514 nm laser light for 5 ms at 5 kW/cm^2. The fit of the histogram revealed an off-rate of 230 ± 40 ms.

cellular background is to use total-internal reflection (TIR) for excitation, which significantly reduces the excited volume (Sako et al., 2000; Funatsu et al., 1995). One disadvantage of TIR is that the excitation intensity at the position of the molecule is difficult to know given that the membrane topology of most cells has a variance of 150 nm or more (Giebel et al., 1999). That might result in >95% fluctuation in the excitation intensity of the evanescent field, which provides the analysis of signal amplitude of signal fluorophores to be prohibitive. A second possibility to reduce the background signal is utilization of time gating of the signal using fluorophores with a fluorescence lifetime much longer than those of flavins (Wilkerson et al., 1993; Lacoste et al., 2000). A third possibility is a short photobleaching treatment with an intense light pulse before the actual experiment (Harms et al., submitted for publication). Although those procedures can significantly reduce the autofluorescence background, a more detailed characterization of the flavin fluorescence is desired for a further optimization and for situations where those experimental treatments are not useful. A spectral comparison of flavinoid and the various autofluorescent proteins (XFPs) is shown in Fig. 9. The absorption spectrum of flavinoid strongly overlaps the excitation spectra of eCFP and eGFP (Fig. 8 *A*), whereas the emission spectrum overlaps most strongly with that of eYFP (Fig. 8 *B*), and minor with that of eCFP and eGFP. For quantification of that observation we define the detection ratio, *R*, describing the relative detection yields of the various XFPs and that of flavinoid (F),

$$R = \frac{\eta_{\mathrm{XFP}}\sigma_{\mathrm{XFP}}(\lambda_{\mathrm{XFP}})}{\eta_{\mathrm{F}}^{\mathrm{XFP}}\sigma_{\mathrm{F}}(\lambda_{\mathrm{XFP}})},$$

for given detection efficiencies, η, and absorption cross sections $\sigma(\lambda)$. Values of $R = 1.8$ for eCFP, $R = 8.7$ for eGFP, $R = 405$ for eYFP, and $R > 10^4$ for DsRed are determined. Hence, from the detection-ratio point of view, DsRed seems far superior to all other autofluorescent proteins. However, the factor of greater than ten photobleaching rate of DsRed in comparison to eYFP is currently limiting its use for single-molecule studies. Thus, for single-molecule studies in vivo, the best fluorescent protein for now is eYFP. It combines a high emission rate, the best resistance to photobleaching, and a high detection ratio with excitation at 514 nm. We also note that the best possible alternative is eGFP in terms of photostability and brightness for utilization in single-molecule in vitro studies in which the background fluorescence is controlled more easily. The newly found DsRed might be attractive alternative for eYFP due to its high count-rate and detection values. Given the parameters reported here, experiments can be optimized for its use. However, utilization of eGFP for single-molecule in vivo studies will be largely obstructed by its low detection ratio with respect to the flavinoid fluorescence.

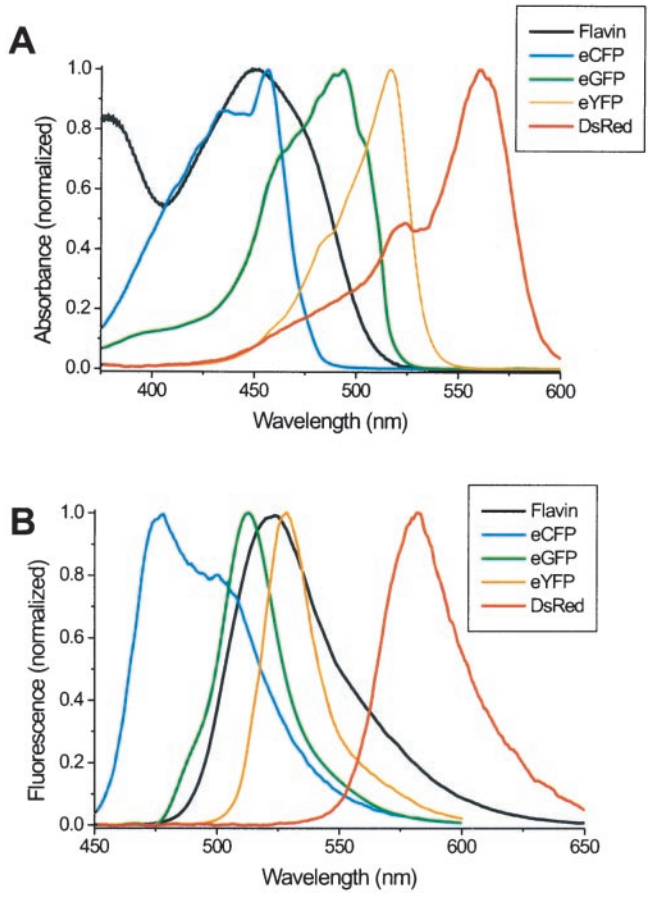

FIGURE 9 Spectral comparison of flavin-di-nucleotide to the fluorescent proteins. (*A*) Normalized absorption spectra. (*B*) Normalized emission spectra.

In summary, we have demonstrated in this article the detection and imaging of single autofluorescent proteins and characterized them in various biocompatible in vitro environments. To date it appears that eYFP is likely a superior choice for applications in dynamics of individually labeled fluorescent fusion proteins. This is due to its brightness, resistance to photobleaching, and detection ratio. In particular, when it is desirable to obtain extended image sequences of the same molecule, in, e.g., single-particle tracking, conformational dynamics, and fluorescence resonance energy transfer, the higher photostability of eYFP will prove vital. It must be noted, however, that in vivo experiments with individual eYFP are still a challenging task. Further research and technological advancements are needed before the exciting combination of recombinant protein technology and single-molecule fluorescence microscopy will answer pending biological questions.

We thank Prof. Dr. H. P. Spaink, University of Leiden, for stimulation and support of the genetic aspects of this research. We also thank Dr. N. M. Soldatov for providing us with samples of DsRed and for support in this

research. We thank W. Jansen van de Laak and E. Gevers for help in data collection and analysis.

This work was supported by generous funds from the Dutch ALW/FOM/NWO program for Physical Biology (to T.S.). L.C. acknowledges support from DGA/DSP (France) and the European Marie-Curie fellowship program.

REFERENCES

Baird, G. S., D. A. Zacharias, and R. Y. Tsien. 2000. Biochemistry, mutagenesis, and oligomerization of DsRed, a red fluorescent protein from coral. *PNAS USA.* 97:11984–11989.

Basché, T., S. Kummer, and C. Bräuchle. 1995. Direct spectroscopic observation of quantum jumps of a single-molecule. *Nature.* 373: 132–134.

Basché, T., W. E. Moerner, M. Orrit, and H. Tallon. 1992. Photon antibunching in the fluorescence of a single dye molecule trapped in a solid. *Phys. Rev. Lett.* 69:1516–1519.

Benson, R. C., R. A. Meyer, M. E. Zaruba, and G. M. McKhann. 1979. Cellular autofluorescence: is it due to flavins? *J. Histochem. Cytochem.* 27:44–48.

Bruchez, Jr., M., M. Moronne, P. Gin, S. Weiss, and A. P. Alivisatos. 1998. Semiconductor nanocrystals as fluorescent biological labels. *Science.* 281:2013–2016.

Chan, W. C., and S. Nie. 1998. Quantum dot bioconjugates for ultrasensitive nonisotopic detection. *Science.* 281:2016–2018.

Chandrasekar, S. 1943. Stochastic problems in physics and astronomy. *Rev. Mod. Phys.* 15:1–36.

Creemers, T. M., A. J. Lock, V. Subramaniam, T. M. Jovin, and S. Volker. 1999. Three photoconvertible forms of green fluorescent protein identified by spectral hole-burning. *Nat. Struct. Biol.* 6:557–560.

De Giorgi, F., Z. Ahmed, C. Bastianutto, M. Brini, L. S. Jovaville, R. Marsault, M. Murgiu, P. Pinton, T. Pozzac, and R. Rizzuto. 1999. Targeting GFP to organelles. *Methods Cell Biol.* Academic Press, San Diego. 58:75–85.

Demtröder, W. 1988. Laser Spectroscopy. Springer, Berlin.

Dickson, R. M., A. B. Cubitt, R. Y. Tsien, and W. E. Moerner. 1997. On/off blinking and switching behaviour of single molecules of green fluorescent protein. *Nature.* 388:355–358.

Edidin, M. 1987. Fluorescent labeling of cell surfaces. *Curr. Top. Membr. Trans.* 29:91–127.

Eigen, M., and R. Rigler. 1994. Sorting single molecules: application to diagnostics and evolutionary biotechnology. *Proc. Natl. Acad. Sci. USA.* 91:5740–5747.

Funatsu, T., Y. Harada, M. Tokunaga, K. Saito, and T. Yanagida. 1995. Imaging of single fluorescent molecules and individual ATP turnovers by single myosin molecules in aqueous solution. *Nature.* 374:555–559.

Garcia-Parajo, M. F., J. A. Veerman, G. M. Segers-Nolten, B. G. de Grooth, J. Greve, and N. F. van Hulst. 1999. Visualising individual green fluorescent proteins with a near field optical microscope. *Cytometry.* 36:239–246.

Giebel, K., C. Bechinger, S. Herminghaus, M. Riedel, P. Leiderer, U. Weiland, and M. Bastmeyer. 1999. Imaging of cell/substrate contacts of living cells with surface plasmon resonance microscopy. *Biophys. J.* 76:509–516.

Griffin, B. A., S. R. Adams, and R. Y. Tsien. 1998. Specific covalent labeling of recombinant protein molecules inside live cells. *Science.* 281:269–272.

Harms, G. S., M. Sonnleitner, G. J. Schütz, H. J. Gruber, and T. Schmidt. 1999. Single-molecule anisotropy imaging. *Biophys. J.* 77:2864–2870.

Hauglund, R. P. 1996. Handbook of Fluorescent Probes and Research Chemicals. Molecular Probes, Eugene, Oregon.

Heikal, A. A., S. T. Hess, G. S. Baird, R. Y. Tsien, and W. W. Webb. 2000. Molecular spectroscopy and dynamics of intrinsically fluorescent proteins: coral red (dsRed) and yellow (Citrine). *Proc. Natl. Acad. Sci. USA.* 97:11996–12001.

Hirschfeld, T. 1976. Optical microscopic observation of single small molecules. *Appl. Opt.* 15:2965–2966.

Holtrup, F. O., G. R. J. Müller, H. Quante, S. Defeyter, F. C. DeSchryver, and K. Müllen. 1997. Terrylenimides: New NIR fluorescent dyes. *Chemistry: A European Journal.* 3:219–225.

Iwane, A. H., T. Funatsu, Y. Harada, M. Tokunaga, O. Ohara, S. Morimoto, and T. Yanagida. 1997. Single molecular assay of individual ATP turnover by a myosin-GFP fusion protein expressed in vitro. *FEBS Lett.* 407:235–238.

Jakobs, S., V. Subramian, A. Schönle, T. M. Jovin, and S. W. Hell. 2000. EFGP and DsRed expressing cultures of *Escherichia coli* imaged by confocal, two-photon and fluorescence lifetime microscopy. *FEBS Lett.* 24012:1–5.

Jung, G., S. Mais, A. Zumbusch, and C. Bräuchle. 2000. The role of dark states in the photodynamics of the green fluorescent protein examined with two-color fluorescence excitation spectroscopy. *J. Phys. Chem. A.* 104:873–877.

Kneen, M., J. Farinas, and A. S. Verkman. 1998. Green fluorescent protein as a noninvasive intracellular pH indicator. *Biophys. J.* 74:1591–1599.

Kubitscheck, U., O. Kuckmann, T. Kues, and R. Peters. 2000. Imaging and tracking of single GFP molecules in solution. *Biophys. J.* 78:2170–2179.

Lacoste, T. D., X. P. Michalet, F. Pinaud, D. S. Chemla, A. P. Alivisatos, and S. Weiss. 2000. Ultrahigh-resolution multicolor colocalization of single fluorescent probes. *Proc. Natl. Acad. Sci. U.S.A.* 97:9461–9466.

Lakowicz, J. R. 1999. Principles of Fluorescence Spectroscopy. Kluwer, New York.

Matz, M. V., A. F. Fradkov, Y. A. Labas, A. P. Savitsky, A. G. Zaraisky, M. L. Markelov, and S. A. Lukyanov. 1999. Fluorescent proteins from nonbioluminescent Anthozoa species. *Nat. Biotech.* 17:969–973.

Miyawaki, A., J. Llopis, R. Heim, J. M. Mccaffery, J. A. Adams, M. Ikura, and R. Y. Tsien. 1997. Fluorescent indicators for Ca^{2+} based on green fluorescent proteins and calmodulin. *Nature.* 388:882–887.

Moriyoshi, K., L. J. Richards, C. Akazawa, D. D. O'Leary, and S. Nakanishi. 1996. Labeling neural cells using adenoviral gene transfer of membrane-targeted GFP. *Neuron.* 16:255–260.

Ormo, M., A. B. Cubitt, K. Kallio, L. A. Gross, R. Y. Tsien, and S. J. Remington. 1996. Crystal structure of the Aequorea victoria green fluorescent protein. *Science.* 273:1392–1395.

Peterman, E. J. G., S. Brasselet, and W. E. Moerner. 1999. The fluorescence dynamics of single molecules of green fluorescent protein. *J. Phys. Chem. A.* 103:10553–10560.

Piston, D. W., G. H. Patterson, and S. M. Knobel. 1999. Quantitative imaging of the green fluorescent protein (GFP). *Methods Cell Biol.* 58:31–48.

Rinia, H. A., R. A. Kik, R. A. Demel, M. M. Snel, J. A. Killian, J. P. Der Eerden, and B. de Kruijff. 2000. Visualization of highly ordered striated domains induced by transmembrane peptides in supported phosphatidylcholine bilayers. *Biochemistry.* 39:5852–5858.

Sako, Y., S. Minoghchi, and T. Yanagida. 2000. Single-molecule imaging of EGFR signaling on the surface of living cells. *Nat. Cell Biol.* 2:168–172.

Saxton, M. J., and K. Jacobson. 1997. Single-particle tracking: applications to membrane dynamics. *Annu. Rev. Biophys. Biomol. Struct.* 26: 373–399.

Schmidt, T., G. J. Schütz, W. Baumgartner, H. J. Gruber, and H. Schindler. 1995. Characterization of photophysics and mobility of single molecules in a fluid lipid membrane. *J. Phys. Chem.* 99:17662–17668.

Schmidt, T., G. J. Schütz, W. Baumgartner, H. J. Gruber, and H. Schindler. 1996. Imaging of single molecule diffusion. *Proc. Natl. Acad. Sci. U.S.A.* 93:2926–2929.

Schütz, G. J., G. Kada, V. P. Pastushenko, and H. Schindler. 2000. Properties of lipid microdomains in a muscle cell membrane visualized by single molecule microscopy. *EMBO J.* 19:892–901.

Schwille, P., U. Haupts, S. Maiti, and W. W. Webb. 1999. Molecular dynamics in living cells observed by fluorescence correlation spectroscopy with one- and two-photon excitation. *Biophys. J.* 77:2251–2265.

Schwille, P., S. Kummer, A. A. Heikal, W. E. Moerner, and W. W. Webb. 2000. Fluorescence correlation spectroscopy reveals fast optical excita-

tion-driven intramolecular dynamics of yellow fluorescent proteins. *Proc. Natl. Acad. Sci. U.S.A.* 97:151–156.

Sullivan, K. F., and S. A. Kay, eds. 1999. Green fluorescent proteins. *Methods Cell Biol.* 58:1–369.

Swaminathan, R., C. P. Hoang, and A. S. Verkman. 1997. Photobleaching recovery and anisotropy decay of green fluorescent protein GFP-S65T in solution and cells: cytoplasmic viscosity probed by green fluorescent protein translational and rotational diffusion. *Biophys. J.* 72:1900–1907.

Tsien, R. Y. 1989. Fluorescent probes of cell signaling. *Annu. Rev. Neurosci.* 12:227–253.

Tsien, R. Y. 1998. The green fluorescent protein. *Annu. Rev. Biochem.* 67:509–544.

Weiss, S. 1999. Fluorescence spectroscopy of single biomolecules. *Science.* 283:1667–1695.

Widengren, J., B. Terry, and R. Rigler. 1999. Protonation kinetics of GFP and FITC investigated by FCS: aspects of the use of fluorescent indicators for measuring pH. *Chem. Phys.* 249:259–271.

Wilkerson, Jr., C. W., P. M. Goodwin, W. P. Ambrose, J. C. Martin, and R. A. Keller. 1993. Detection and lifetime measurement of single molecules in flowing sample streams by laser-induced fluorescence. *Appl. Phys. Lett.* 62:2030–2032.

Zuhlke, R. D., G. S. Pitt, K. Deisseroth, R. W. Tsien, and H. Reuter. 1999. Calmodulin supports both inactivation and facilitation of L-type calcium channels. *Nature.* 399:159–162.